International Journal of Scientific Engineering and Science
Volume 10, Issue 5, pp. 31-43, 2026. ISSN (Online): 2456-7361

Characterization of Natural Radioactivity from the ^{238}U Series, ^{232}Th Series, and ^{40}K in Soils of Vohémar District, Madagascar

VELOSON Sahidivola Hervé[1], DONNE Zafizara[1], NGOKO Fidelin[1], RANDRIA Felix[1], LEMA Marnella Quetty[2], RASOLONIRINA Martin[3], KALL Briant[1]
[1]Department of Nuclear Metrology and Environment, Faculty of Science, University of Antsiranana, Madagascar
[2]Department of Engineering in Sciences and Water Techniques, Faculty of Sciences, University of Antananarivo, Madagascar
[3]Department of Nuclear Techniques and Analysis, National Institute of Sciences and Nuclear Techniques, Madagascar

Abstract *— This study presents the first comprehensive characterization of natural radioactivity in the soils of the Vohémar district, located in the SAVA region of northeastern Madagascar. The primary objective was to quantify the specific activities of radionuclides from the ^{238}U and ^{232}Th decay series, as well as ^{40}K, to establish a radiological database for this area of high mining potential. Twenty-one (21) soil samples, representative of the district's geo-pedological diversity, were analyzed by gamma spectrometry using a NaI(Tl) scintillation detector. The results reveal mean specific activities of 74 ± 13 Bq/kg for ^{238}U, 78 ± 6 Bq/kg for ^{232}Th, and 484 ± 57 Bq/kg for ^{40}K. These values are significantly higher than the UNSCEAR world averages, with uranium and thorium levels being 2.1 and 2.6 times higher in Vohémar, respectively. Spatial analysis shows strong heterogeneity: the highest concentrations are clustered in the western and central parts, correlated with the Precambrian crystalline basement (Bemarivo belt) and plutonic intrusions. Conversely, coastal and eastern areas exhibit lower levels due to sedimentary dilution and intense potassium leaching under a tropical climate. The lack of a linear correlation among the three radionuclides confirms that distinct geochemical mechanisms govern their distributions. This work constitutes an essential reference for environmental management and radiation protection for local populations.*

Keywords—*Natural Radioactivity, Gamma-ray Spectrometry, Soils, Spatial Distribution, Geochemistry, District of Vohémar, Madagascar.*

I. INTRODUCTION

Environmental radioactivity is a ubiquitous natural phenomenon that constitutes the radiological background of the biosphere. Human exposure to this radioactivity primarily originates from cosmic radiation and primordial radionuclides present in the Earth's crust since its formation. Among the latter, potassium-40 (^{40}K), as well as the decay series of uranium-238 (^{238}U) and thorium-232 (^{232}Th), are the main contributors to the terrestrial gamma radiation dose received by populations (Singh *et al.,* 2005; Kall *et al.,* 2014; Amanjeet *et al.,* 2017; Durusoy & Yildirim, 2017; Stolerie *et al.,* 2021; Rahelivao *et al.,* 2023; Ngoko *et al.,* 2024; Tsilailay *et al.,* 2025; Najam *et al.,* 2025; Chakma *et al.,* 2026).

The distribution of these elements in soils is governed by their intrinsic geochemical properties and the lithological nature of the substrate (Adabanija *et al.,* 2020; Najam *et al.,* 2025; Djaovagnono *et al.,* 2025; Tsilailay *et al.,* 2025). Uranium and thorium are incompatible lithophile elements that tend to concentrate in acidic and differentiated magmatic rocks. However, their post-crystallization behavior differs radically: uranium is chemically mobile under oxidizing conditions and can be transported as soluble uranyl ions (UO_2^{2+}) (IRSN & INRS, 2014), whereas thorium (Th^{4+}) is extremely stable, poorly soluble, and generally remains trapped in resistant accessory minerals such as monazite (IRSN & INRS, 2013; Donné et al., 2021). Potassium, for its part, is a major element in feldspars and micas. Unlike U and Th, potassium (K^+) is a highly mobile and bioavailable ion, particularly sensitive to chemical leaching processes under humid tropical climates (Donné *et al.,* 2021; Stolerie *et al.,* 2021).

Although these sources are of natural origin, local geological variability can lead to significantly high concentrations in certain regions, notably those characterized by granitic rocks (Singh *et al.,* 2005; Adabanija *et al.,* 2020) or mineralized sands rich in monazite and zircon (Rafidimanantsoa *et al.,* 2021; Chakma *et al.,* 2026). In addition to this natural contribution, anthropogenic sources related to industrial and extractive activities can concentrate these radionuclides, thereby increasing the risk of radiological exposure for local populations (Rafidimanantsoa *et al.,* 2021; Kanmi *et al.,* 2025).

Due to the complexity of its geological basement, Madagascar hosts significant radioactive mineral resources. While the study of environmental radioactivity holds economic interest for inventorying potential uranium and thorium sites for a future energy transition, it primarily addresses a major public health imperative (Rabesiranana, 2017; Donné *et al.,* 2021; Ngoko *et al.,* 2024). It is this latter aspect that mainly motivates the present study.

Indeed, owing to the high penetrating power of gamma radiation and its interactions at the cellular level, chronic exposure to radionuclides from the ^{238}U and ^{232}Th series which exhibit both radiological and chemical toxicity can induce adverse effects on public health (IRSN & INRS, 2013 and 2014; Randriamora *et al.*, 2017; Donné *et al.,* 2021; Rahelivao *et al.,* 2023). Therefore, it is essential to evaluate the spatial distribution of these natural radionuclides in soils to estimate health risks and establish adequate radiation protection

International Journal of Scientific Engineering and Science
Volume 10, Issue 5, pp. 31-43, 2026. ISSN (Online): 2456-7361

measures (Ngoko *et al.,* 2024; Kanmi *et al.,* 2025; Najam *et al.,* 2025; Chakma *et al.,* 2026).

In this context, the SAVA region, and specifically the Vohémar district, is attracting increasing interest due to its mining potential, notably marked by gold mining and the presence of black sands (heavy minerals) likely to harbor radioactive elements. However, data regarding environmental radioactivity levels in this area remain highly fragmentary, although recent studies have begun to document neighboring districts such as Antsiranana II, Ambilobe, and Antalaha (Tsilailay *et al.,* 2025; Stolerie *et al.,* 2021; Ngoko *et al.,* 2024). The lack of precise radiological mapping significantly limits the assessment of risks associated with the prolonged exposure of resident populations.

To address this gap, this study aims to evaluate, via gamma spectrometry, the specific activities of radionuclides from the ^{238}U and ^{232}Th series, as well as ^{40}K, in the soils of the Vohémar district. The objective is not only to characterize the natural radiological background of this district but also to provide essential reference data for the establishment of a national natural radioactivity map in Madagascar.

II. Material and Methods

2.1. Study Area Description

The study was conducted in the Vohémar District, situated along the northeastern coast of Madagascar within the SAVA Region. The district is bordered by the districts of Sambava to the south, Ambilobe to the west, and Antsiranana II to the north. It lies between latitudes 12°43′06.17"–14°01′20.20" S and longitudes 49°21′19.74"–50°11′15.19" E, covering a total area of 8,268.55 km².

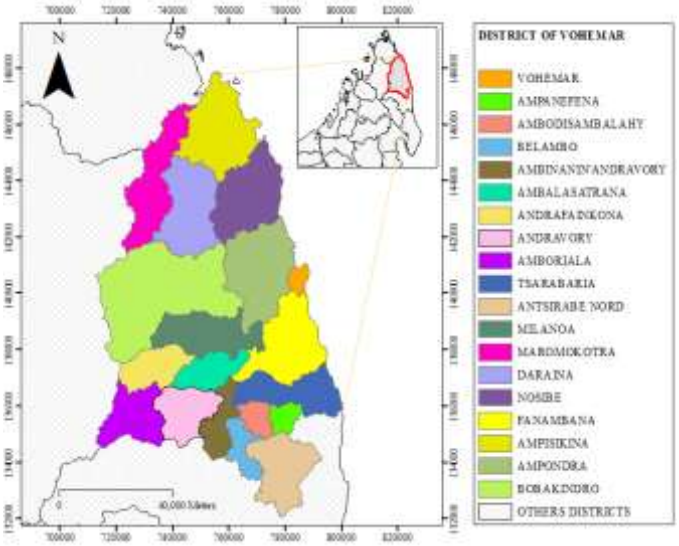

Fig. 1. Location of Study Area

The region is characterized by a tropical climate with a marked alternation between a humid season, concentrated from January to March, and a relatively dry season extending from April to November. Temperatures are generally high, with monthly averages ranging between 23°C and 27°C. Observed extreme values fluctuate from 15.3°C to 35.1°C, reflecting a moderate thermal amplitude. Annual rainfall varies between 935 mm and 2,255 mm with an average of 1,445 mm, reflecting significant interannual variability and confirming the influence of oceanic air masses and cyclonic events on this coastal zone (Schreurs & Rakotoarisoa, 2011).

Administratively, the district is divided into 19 communes: Ambalasatrana, Ambinanin'andravory, Amboriala, Ampanefena, Ampisikina, Ampondra, Andrafainkona, Andravory, Ambodisambalahy, Antsirabe Nord, Belambo, Bobakindro, Daraina, Fanambana, Maromokotra, Milanoa, Nosibe, Tsarabaria, and Vohemar, which also serves as its administrative center. In 2020, the district's population was estimated at 264,236 inhabitants.

From a geological perspective, the framework of the Vohemar district is highly diverse and is primarily underlain by a Precambrian basement forming part of the northern Bemarivo Belt. This basement consists predominantly of Neoproterozoic metamorphic plutonic rocks of the Manambato suite, accompanied by metasedimentary rocks of the Daraina Group. Approximately 20 kilometers south of Vohemar, Cretaceous plutonic rocks of the Analalava suite intrude into this Precambrian basement, which is also intersected by north-northwest to south-southeast trending Cretaceous dike swarms. Furthermore, a narrow strip of Cretaceous continental sediments is present along the eastern margin of the basement. More recent geological activity is represented by Neogene and potentially Quaternary volcanic rocks, including basalts and rhyolites, which have extruded mainly south of the town. The coastal and riverine landscapes are shaped by Quaternary dune systems running parallel to the shoreline, alluvial deposits flanking the main east-west-oriented rivers, as well as extensive intertidal coral reefs and lagoons. This complex geological history endows the hinterland of Vohemar with a wide variety of mineral resources. These include large ultramafic lenses containing chlorite-schist or soapstone, pure quartz deposits, and coastal dune sands with high concentrations of iron-titanium oxide known as ilmenite. Additionally, the region hosts copper, barium, and barite occurrences associated with Neogene basalts, alongside significant primary and alluvial deposits of gold, silver, tin, and lead (Schreurs & Rakotoarisoa, 2011).

2.2. Sampling Strategy and Sample Preparation Protocols

Data collection was conducted during a soil sampling campaign in October 2023, during which 21 samples were collected to accurately represent the geo-pedological variability of the Vohémar district. The selection of sampling sites was guided by geological diversity and land use patterns, including agricultural, forested, coastal, and urban areas, while accounting for the intensity of local anthropogenic activities. Each sampling point was precisely georeferenced using a Garmin GPS, enabling the generation of a rigorous map in ArcGIS 10.5 based on data from the Foiben-Taosarintanin'i Madagasikara (Fig. 2).

At each location, approximately 300 g of soil was extracted from a depth of 30 cm after the removal of surface litter, and the samples were coded from ECH-01 to ECH-21 before being

International Journal of Scientific Engineering and Science
Volume 10, Issue 5, pp. 31-43, 2026. ISSN (Online): 2456-7361

transported to the laboratory of the National Institute of Nuclear Sciences and Techniques for processing.

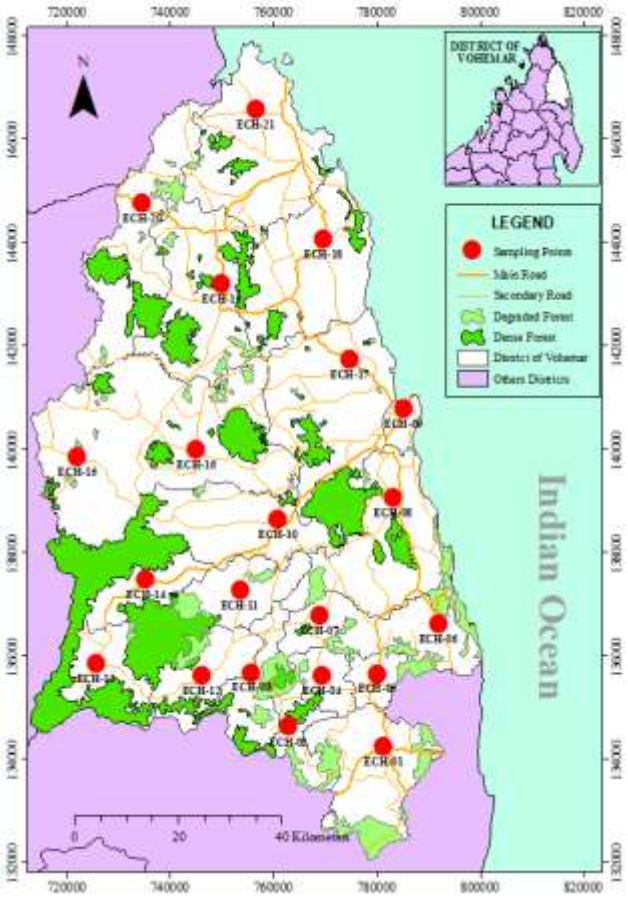

Fig. 2. Location of sampling points

Physical preparation consisted of oven-drying at 105 °C until a constant weight was achieved, followed by grinding and sieving to less than 2 mm to ensure powder homogeneity, which was then sealed in 100 cm³ cylindrical polyethylene containers and stored for three weeks to establish secular equilibrium between ^{226}Ra and its short-lived progeny within the ^{238}U decay chain.

2.3. Gamma-ray Spectrometry Measurement

The specific activities of ^{238}U, ^{232}Th, and ^{40}K were determined by gamma spectrometry with a 3" × 3" NaI(Tl) scintillation detector and an ORTEC digiBase acquisition unit. Ambient background was mitigated by a cylindrical shield of lead (30 mm) and stainless steel (10 mm), yielding an energy resolution of 7.5% at 1332.5 keV. Samples were counted for 12 hours, and background was subtracted using blank container measurements. Activity quantification relied on the spectrum stripping technique (Chiozzi et al., 2000) with 15% widened energy windows centered at 1461 keV (^{40}K), 1764.5 keV (^{214}Bi), and 2614.5 keV (^{208}Tl) (Fig. 3). The method was validated using IAEA standards RGK-1, RGU-1, and RGTh-1, consistent with established protocols (Chiozzi *et al.*, 2000; Tzortzis *et al.*, 2003; Cinelli *et al.*, 2016; Stolerie *et al.*, 2021; Rahelivao *et al.*, 2023; Ngoko *et al.*, 2024).

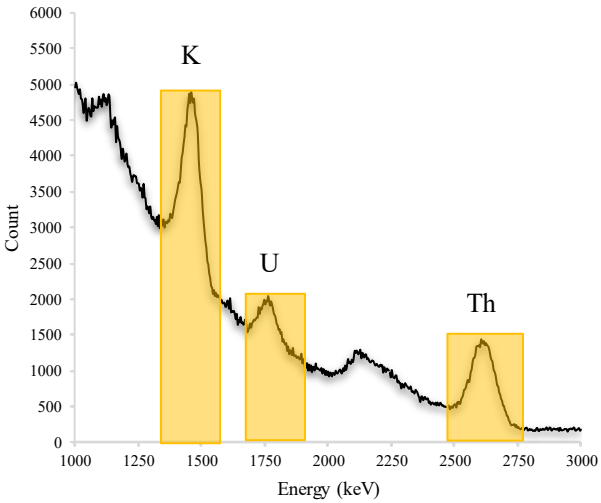

Fig. 3. Energy windows used to quantify ^{40}K, ^{238}U, and ^{232}Th

2.4. Modeling of Detection Efficiency Constants and Analytical Calibration

The determination of efficiency constants is based on modeling the linear relationship between the net count rate observed in a specific region of interest and the activity of each radionuclide present in the standard. The net count rate for each energy window is obtained by subtracting the ambient background rate from the total number of counts recorded per unit of time for each reference standard. By utilizing measurements performed on the IAEA-certified standards, an efficiency matrix was constructed to isolate the respective contributions of each isotope and to quantify the detection coefficients specific to each region of interest. For standards presenting complex spectra, the constants were calculated through a successive resolution of mathematical equations to correct for interferences and overlaps between the uranium and thorium energy windows.

The net count rate $R_{i,j}$ observed in a region of interest (ROI) i for a given standard source j, depends on the activities $A_{n,j}$ of each radionuclide n present in the standard. This relationship is expressed by the following equation (Chiozzi *et al.*, 2000; Stolerie *et al.*, 2021; Rahelivao *et al.*, 2023; Ngoko *et al*, 2024; Djaovagnono *et al*, 2025; Tsilailay *et al.*, 2025):

$$R_{i,j} = \sum_{n=1}^{3} e_{i,n} \times A_{n,j} \qquad (1)$$

Where the indices i, j, and n (ranging from 1 to 3) respectively denote the regions of interest (1: K, 2: U, 3: Th), identifies the standard source (RGK-1, RGU-1, and RGTh-1), and corresponds to the radionuclide (^{40}K, ^{238}U, ^{232}Th). $e_{i,n}$ is the detection efficiency for radionuclide n in ROI i. The net count rate is calculated using the following formula:

$$R_{i,j} = \frac{N_{i,j}}{t_j} - B_i \qquad (2)$$

International Journal of Scientific Engineering and Science
Volume 10, Issue 5, pp. 31-43, 2026. ISSN (Online): 2456-7361

Where $N_{i,j}$ is the number of recorded counts in in ROI i for the standard j; t_j is the counting time for standard j; and B_i is the background count rate in ROI i.

Using Equation (1), an efficiency matrix (E) can be constructed, relating the net count rates in each ROI to the actual activities of the radionuclides in the standards.

For the RGK-1 standard, which mainly contains potassium, only the activity of ^{40}K is significant. The efficiency constant, representing the detection efficiency of ^{40}K in the K window, is calculated as:

$$e_{1,1} = \frac{R_{1,1}}{A_{1,1}} \tag{3}$$

For the RGU-1 standard, the efficiency constants $e_{1,2}$ and $e_{2,2}$ were quantified using Equation (4):

$$e_{1,2} = \frac{R_{1,2}}{A_{2,2}} \quad \text{and} \quad e_{2,2} = \frac{R_{2,2}}{A_{2,2}} \tag{4}$$

For the RGTh-1 standard, Equations (5) and (6) were used to determine the efficiency constants $e_{1,3}$, and $e_{2,3}$:

$$e_{1,3} = \frac{1}{A_{3,3}}\left(R_{1,3} - \frac{A_{2,3}}{A_{2,2}}R_{1,2}\right) \tag{5}$$

$$e_{2,3} = \frac{1}{A_{3,3}}\left(R_{2,3} - \frac{A_{2,3}}{A_{2,2}}R_{2,2}\right) \tag{6}$$

The constants $e_{3,2}$ and $e_{3,3}$ are determined by combining the uranium and thorium count rates in the third region of interest, as follows:

$$e_{3,2} = \frac{R_{3,2}}{A_{2,2}} \quad \text{and} \quad e_{3,3} = \frac{1}{A_{3,3}}\left(R_{3,3} - \frac{A_{2,3}}{A_{2,2}}R_{3,2}\right) \tag{7}$$

2.5. Specific Activity Calculation and Uncertainty Assessment

The calculation of final specific activities is performed through the inversion of the efficiency matrix, which allows the measured net count rates to be linked to the initially unknown activities of the radionuclides within the soil samples. This methodological step establishes a system of linear equations where the activity of each isotope is deduced from a weighted combination of the count rates recorded in the three spectral windows defined during calibration. Uncertainties associated with the calculated activities were rigorously evaluated using the law of error propagation, integrating both the statistical uncertainty of the count rates and the uncertainty regarding the coefficients of the inverse matrix.

The net count rates (R) for each region of interest are linked to radionuclide activities (A) via the matrix equation (Stolerie *et al.,* 2021; Rahelivao *et al.,* 2023; Ngoko *et al,* 2024; Djaovagnono *et al,* 2025; Tsilailay *et al.,* 2025):

$$R = E \,.\, A \tag{8}$$

Where R is the vector of net count rates (R_K, R_U, R_{Th}); E is the efficiency matrix (3 x 3) determined during calibration, and A is the vector of unknown activities (A_K, A_U, A_{Th}). This can be written as (Stolerie et al., 2021; Rahelivao *et al.,* 2023; Ngoko *et al*, 2024; Djaovagnono *et al,* 2025; Tsilailay *et al.,* 2025):

$$\begin{pmatrix} R_K \\ R_U \\ R_{Th} \end{pmatrix} = \begin{pmatrix} e_{1,1} & e_{1,2} & e_{1,3} \\ 0 & e_{2,2} & e_{2,3} \\ 0 & e_{3,2} & e_{3,3} \end{pmatrix} \begin{pmatrix} A_K \\ A_U \\ A_{Th} \end{pmatrix} \tag{9}$$

To determine A, the equation is inverted:

$$\begin{pmatrix} A_K \\ A_U \\ A_{Th} \end{pmatrix} = \begin{pmatrix} a_{1,1} & a_{1,2} & a_{1,3} \\ 0 & a_{2,2} & a_{2,3} \\ 0 & a_{3,2} & a_{3,3} \end{pmatrix} \begin{pmatrix} R_K \\ R_U \\ R_{Th} \end{pmatrix} \tag{10}$$

This results in the following system of equations, where the coefficients $a_{i,j}$ are the elements of E^{-1}, the inverse of matrix E (Stolerie *et al.,* 2021; Rahelivao *et al.*, 2023; Ngoko *et al,* 2024; Djaovagnono *et al,* 2025; Tsilailay *et al.,* 2025):

$$\begin{cases} A_K = a_{1,1}R_K + a_{1,2}R_U + a_{1,3}R_{Th} \\ A_U = a_{2,2}R_U + a_{2,3}R_{Th} \\ A_{Th} = a_{3,2}R_U + a_{3,3}R_{Th} \end{cases} \tag{11}$$

Knowing that the constants of the inverse matrix E^{-1} must be expressed in terms of the efficiency constants $e_{i,n}$ in the three regions of interest.

Where

$$a_{1,1} = \frac{1}{e_{1,1}} \tag{12}$$

$$a_{1,2} = \frac{e_{1,2}e_{3,3} - e_{1,3}e_{3,2}}{e_{1,1}\left(e_{2,3}e_{3,2} - e_{2,2}e_{3,3}\right)} \tag{13}$$

$$a_{1,3} = \frac{e_{1,3}e_{2,2} - e_{1,2}e_{2,3}}{e_{1,1}\left(e_{2,3}e_{3,2} - e_{2,2}e_{3,3}\right)} \tag{14}$$

$$a_{2,2} = \frac{-e_{3,3}}{e_{2,3}e_{3,2} - e_{2,2}e_{3,3}} \tag{15}$$

$$a_{2,3} = \frac{e_{2,3}}{e_{2,3}e_{3,2} - e_{2,2}e_{3,3}} \tag{16}$$

$$a_{3,2} = \frac{e_{2,3}}{e_{2,3}e_{3,2} - e_{2,2}e_{3,3}} \tag{17}$$

$$a_{3,3} = \frac{-e_{2,2}}{e_{2,3}e_{3,2} - e_{2,2}e_{3,3}} \tag{18}$$

Uncertainties in activity were computed using by the law of error propagation. The overall uncertainty for each activity is given by (Stolerie *et al.,* 2021; Rahelivao *et al.,* 2023; Ngoko *et al,* 2024; Djaovagnono *et al,* 2025; Tsilailay *et al.,* 2025):

$$\sigma_{A_n} = \sqrt{\sum_i \left[\left(R_i \times \sigma_{a_{n,i}}\right)^2 + \left(a_{n,i} \times \sigma_{R_i}\right)^2\right]} \tag{19}$$

Where σ_{A_n} is the final uncertainty on the calculated activity for radionuclide n; n is the index for the radionuclide whose activity is being calculated (n = 1 for ^{40}K, n = 2 for ^{238}U, and n = 3 for ^{232}Th); i is the index for each measurement window (i = 1 for the K window, i = 2 for the U window, and i = 3 for the Th window); $\sum_i$ is the summation over all measurement

International Journal of Scientific Engineering and Science
Volume 10, Issue 5, pp. 31-43, 2026. ISSN (Online): 2456-7361

windows i ; $a_{n,i}$ is the coefficient of the inverse matrix that relates activity n to count rate i ; R_i is the net count rate in measurement window i ; $\sigma_{a_{n,i}}$ is the uncertainty on the matrix coefficient $a_{n,i}$; σ_{R_i} is the statistical uncertainty on the net count rate R_i .

The detection limit L_n was calculated using the Currie formula (Kall *et al,* 2014; Djaovagnono *et al,* 2025; Tsilailay *et al.,* 2025):

$$L_n = \frac{2\sqrt{2}}{e_{i,n}} \times \sqrt{\left(\frac{B_i}{t}\right)} \quad (20)$$

Where B_i is the background count, $e_{i,n}$ the efficiency, and t the counting time.

To facilitate interpretation, specific activities (in Bq/kg) were converted into elemental concentrations (in ppm or %) using (Erdi-Krausz *et al.,* 2003; Tzortzis & Tsertos, 2004; Bajoga *et al.,* 2019; Shaba *et al.,* 2024; Djaovagnono *et al,* 2025):

$$1 \text{ ppm U} = 12.35 \text{ Bq.kg}^{-1} \text{ of } {}^{238}U \quad (21)$$

$$1 \text{ ppm Th} = 4.06 \text{ Bq.kg}^{-1} \text{ of } {}^{232}\text{Th} \quad (22)$$

$$1\% \text{ K} = 313 \text{ Bq.kg}^{-1} \text{ of } {}^{40}K \quad (23)$$

Uncertainties on elemental concentrations were propagated from those on specific activities. Accordingly, the elemental concentrations of uranium and thorium are expressed in parts per million (ppm), where 1 ppm equals 1 mg/kg, while potassium concentration is expressed as a percentage (%) due to its significantly higher natural abundance compared to uranium or thorium.

III. Results and Discussion

The specific activities of radionuclides from the ^{238}U and ^{232}Th decay series, as well as ^{40}K, were measured in the 21 soil samples collected from the Vohémar district. Detailed results, accompanied by their statistical analysis and geo-pedological interpretation, are presented below.

3.1. Specific Activities of Natural Radionuclides

Table I presents the specific activities (Bq·kg^{-1}) and elemental concentrations (ppm or %) of the natural radionuclides measured in the 21 soil samples from the Vohémar district. The results reveal a pronounced spatial variability, characteristic of the region's geological diversity.

The specific activities of ^{238}U show a very wide range, extending from (312 ± 3) Bq·kg^{-1} (ECH-18) to a maximum of (221 ± 5) Bq·kg^{-1} (ECH-06). This fluctuation corresponds to equivalent uranium (eU) elemental concentrations ranging from (0.97 ± 0.24) ppm to (17.89 ± 0.40) ppm. The mean specific activity for the entire district is (74.43 ± 12.94) Bq·kg^{-1} (equivalent to a mean concentration of (6.03 ± 1.05) ppm). Comparing these results to the global average values reported by UNSCEAR (2000), which are 35 Bq·kg^{-1} or 2.83 ppm, the average in Vohémar district is more than twice the world average. Sample ECH-06 exceeds this standard by a factor of six, indicating areas of exceptional uranium enrichment.

TABLE I. Specific activities and elemental concentrations of natural radionuclides in volcanic soils of the Vohemar District

Locality	Sample No	Laborde Coordination (m)		Specific activity (Bq/kg)			Elemental concentration (ppm)		
		Longitude	Latitude	^{238}U	^{232}Th	^{40}K	eU	eTh	K
Antsirabe Nord	ECH-01	781369.08	1342311.10	46 ± 5	111 ± 6	416 ± 11	3.72 ± 0.40	27.34 ± 1.48	1.33 ± 0.04
Belambo	ECH-02	762954.91	1346147.39	196 ± 6	80 ± 6	332 ± 11	15.87 ± 0.49	19.70 ± 1.48	1.06 ± 0.04
Ambinanin'andravory	ECH-03	755793.85	1356633.23	18 ± 4	66 ± 6	734 ± 17	1.46 ± 0.32	16.26 ± 1.48	2.35 ± 0.05
Ambodisambalahy	ECH-04	769348.72	1356121.72	57 ± 5	110 ± 6	183 ± 9	4.62 ± 0.40	27.09 ± 1.48	0.58 ± 0.03
Ampanefena	ECH-05	780090.31	1356377.48	50 ± 5	47 ± 5	292 ± 7	4.05 ± 0.40	11.58 ± 1.23	0.93 ± 0.02
Tsarabaria	ECH-06	791854.92	1366096.06	221 ± 5	89 ± 5	137 ± 6	17.89 ± 0.40	21.92 ± 1.23	0.44 ± 0.02
Tsarabaria	ECH-07	768837.22	1367630.57	99 ± 4	51 ± 6	585 ± 16	8.02 ± 0.32	12.56 ± 1.48	1.87 ± 0.05
Fanambana	ECH-08	783159.34	1390392.52	138 ± 5	59 ± 6	660 ± 17	11.17 ± 0.40	14.53 ± 1.48	2.11 ± 0.05
Vohemar	ECH-09	785205.36	1407783.67	15 ± 2	24 ± 4	710 ± 14	1.21 ± 0.16	5.91 ± 0.99	2.27 ± 0.04
Milanoa	ECH-10	760908.90	1386300.49	42 ± 3	39 ± 4	468 ± 10	3.40 ± 0.24	9.61 ± 0.99	1.50 ± 0.03
Ambalasatrana	ECH-11	753492.08	1372489.87	125 ± 3	84 ± 5	832 ± 16	10.12 ± 0.24	20.69 ± 1.23	2.66 ± 0.05
Andravory	ECH-12	746075.27	1356121.72	111 ± 3	86 ± 5	632 ± 13	8.99 ± 0.24	21.18 ± 1.23	2.02 ± 0.04
Amboriala	ECH-13	725615.09	1358423.49	35 ± 4	66 ± 6	156 ± 8	2.83 ± 0.32	16.26 ± 1.48	0.50 ± 0.03
Andrafainkona	ECH-14	735333.67	1374535.88	37 ± 3	71 ± 5	411 ± 9	3.00 ± 0.24	17.49 ± 1.23	1.31 ± 0.03
Bobakindro	ECH-15	722034.56	1398320.84	38 ± 4	75 ± 6	166 ± 8	3.08 ± 0.32	18.47 ± 1.48	0.53 ± 0.03
Bobakindro	ECH-16	745052.26	1399855.36	139 ± 6	65 ± 6	878 ± 18	11.26 ± 0.49	16.01 ± 1.48	2.81 ± 0.06
Ampondra	ECH-17	774719.52	1417246.51	61 ± 5	97 ± 6	147 ± 8	4.94 ± 0.40	23.89 ± 1.48	0.47 ± 0.03
Nosibe	ECH-18	769604.47	1440519.96	12 ± 3	144 ± 5	629 ± 11	0.97 ± 0.24	35.47 ± 1.23	2.01 ± 0.04
Daraina	ECH-19	749911.55	1431824.38	33 ± 3	111 ± 5	1015 ± 18	2.67 ± 0.24	27.34 ± 1.23	3.24 ± 0.06
Maromokotra	ECH-20	734566.42	1447425.27	41 ± 4	105 ± 6	427 ± 12	3.32 ± 0.32	25.86 ± 1.48	1.36 ± 0.04
Ampisikina	ECH-21	756561.11	1465583.68	49 ± 3	61 ± 5	344 ± 8	3.97 ± 0.24	15.02 ± 1.23	1.10 ± 0.03
Mean ± Standard Error of Mean				74 ± 13	78 ± 6	484 ± 57	6.03 ± 1.05	19.25 ± 1.53	1.54 ± 0.18
(Minimal value – maximal value)				(12 – 221)	(24 – 144)	(137 – 1015)	(0.97 – 17.89)	(5.91 – 35.47)	(0.44 – 3.24)
Worldwide mean value (UNSCEAR, 2000) *				35	30	400	2.83	7.39	1.28

* These average values were obtained by converting the worldwide average activity concentrations for ^{238}U (35 Bq/kg), ^{232}Th (30 Bq/kg), and ^{40}K (400 Bq/kg) into their respective elemental concentrations eU (mg/kg), eTh (mg/kg), and K (%) using Equation (14).

For the ^{232}Th series, specific activities range from (24 ± 4) Bq·kg^{-1} (ECH-09) to (144 ± 5) Bq·kg^{-1} (ECH-18). The corresponding equivalent thorium (eTh) elemental concentrations vary from (5.91 ± 0.99) ppm to (35.47 ± 1.23)

ppm. The recorded mean activity is (78.14 ± 6.20) Bq·kg^{-1} or (19.25 ± 1.53) ppm. This mean value is significantly higher than the UNSCEAR (2000) reference of 30 Bq·kg^{-1} or 7.39 ppm. The predominance of thorium in several samples, particularly ECH-18 and ECH-01, highlights the richness of the Vohémar crystalline basement in accessory heavy minerals such as monazite.

^{40}K exhibits the widest range of variation, with activities ranging from (137±6) Bq·kg^{-1} (ECH-06) to (1015 ± 18) Bq·kg^{-1} (ECH-19). In terms of total potassium elemental concentration (K %), this corresponds to contents between (0.44 ± 0.02) % and (3.24 ± 0.06) %. The mean activity of potassium-40 in the district is (483.52 ± 57.37) Bq·kg^{-1} or (1.54 ± 0.18) %. This average is slightly higher than the UNSCEAR (2000) world average of 400 Bq·kg^{-1} or 1.28 %. Interestingly, sample ECH-06, which showed the highest uranium activity, has the lowest potassium content, suggesting opposing geochemical processes of weathering or leaching.

Generally, the mean specific activities of uranium-238 and thorium-232 in Vohémar district are 2.1 and 2.6 times higher than the UNSCEAR (2000) global averages, respectively. This strong radiological signature, coupled with a significant dispersion of values, confirms that the district constitutes a highly radioactive geochemical province, necessitating a thorough analysis of its spatial distribution.

3.2. Descriptive Statistics and Normality Tests

The detailed statistical analysis of the 21 samples (N=21), presented in Table II, characterizes the distribution pattern of natural radionuclides within the Vohémar district.

TABLE II. Statistical distribution of natural radionuclide activities

Statistical parameters	^{238}U	^{232}Th	^{40}K
Number of samples	21	21	21
Minimum	12.00	24.00	137.00
Maximum	221.00	144.00	1015.00
Mode	12.00	66.00	137.00[a]
Mean	74.43	78.14	483.52
Std. Error of Mean	12.94	6.20	57.37
Std. Deviation	59.28	28.43	262.90
Variance	3514.46	808.23	69114.56
25th percentile	36.00	60.00	237.50
50th percentile (Median)	49.00	75.00	427.00
75th percentile	118.00	101.00	685.00
Skewness	1.24	0.31	0.32
Kurtosis	0.72	0.17	-0.87
Test of Normality (Shapiro-Wilk)	0.003	0.965	0.282

Skewness coefficients are positive for all three radionuclides, reaching 1.24 for ^{238}U, 0.31 for ^{232}Th, and 0.32 for ^{40}K, indicating distributions that are systematically skewed towards higher activity values. This positive asymmetry is visually confirmed by the histograms in Fig. 4a, Fig. 4b, and Fig. 4c, which show a higher frequency of samples in the low-to-moderate activity classes. For ^{238}U, the high skewness value coupled with a kurtosis of 0.72 reflects a leptokurtic distribution with a significant tail towards high activities. This implies that the mean of 74.43 Bq·kg^{-1} is strongly influenced by a few extreme values, notably the maximum of 221 Bq·kg^{-1}, thus sitting well above the median value (50th percentile) of 49 Bq·kg^{-1}. Conversely, ^{40}K exhibits a negative kurtosis of -0.87, indicating a platykurtic distribution that is flatter than a normal distribution. The wide range between the minimum of 137 Bq·kg^{-1} and the maximum of 1015 Bq·kg^{-1}, associated with an extremely high variance of 69,114.56, demonstrates much greater data dispersion for potassium compared to the other radionuclides.

The Shapiro-Wilk normality test presented in Table II provides fundamental insights into the geochemical nature of these distributions. For ^{238}U, the p-value of 0.003 is well below the critical threshold of 0.05, necessitating the rejection of the null hypothesis of normality for this radionuclide. This lack of normality is evident in the Normal Q-Q plot (Fig. 5a), where the data points deviate significantly from the theoretical straight line, confirming that uranium is subject to localized enrichment processes creating radiological hotspots. For ^{232}Th, although the mean activity is high, the Shapiro-Wilk test yields a p-value of 0.965, indicating a statistically normal distribution. The histogram in Fig. 4b shows a balanced bell shape, while the Q-Q plot in Fig. 5b presents points perfectly aligned with the theoretical line, suggesting that thorium is relatively homogeneously distributed within the district's rock matrix. ^{40}K, with a p-value of 0.282, also follows a normal distribution despite visible deviations at the extremities of the Q-Q plot (Fig. 5c), illustrating the influence of leaching. Analysis of the percentiles shows that the interquartile range (25th to 75th percentile) is particularly wide for ^{40}K, ranging from 237.50 to 685.00 Bq·kg^{-1}, confirming major spatial heterogeneity. Finally, for uranium, the fact that 75% of the samples have an activity below 118 Bq·kg^{-1} highlights that the maximum value of 221 Bq·kg^{-1} represents an isolated geochemical anomaly relative to the rest of the population.

In general, the statistical analysis reveals two distinct geochemical behaviors: thorium follows a coherent and normal geochemical background, while uranium is characterized by asymmetrical radiological anomalies. The high variance of potassium confirms the predominant impact of chemical weathering processes on the uneven redistribution of elements within the Vohémar district.

3.3. Spatial Distribution Analysis

3.3.1. Analysis of ^{238}U Distribution Relative to the Geological Setting

Examination of Fig. 6a establishes a direct correlation between the specific activities of ^{238}U and the nature of the underlying lithological formations in the Vohémar district. It is observed that the highest uranium levels are systematically located within the Precambrian basement belonging to the Bemarivo belt, as well as in proximity to Cretaceous plutonic intrusions, such as the Analalava suite. This phenomenon is explained by the geochemical behavior of uranium, which, as an incompatible element, tends to concentrate preferentially in acidic and differentiated magmatic rocks, notably the granodiorites and rhyolites present in this central zone. Conversely, areas exhibiting lower activities correspond to more recent sedimentary formations and alluvial deposit zones located along the coastline, where uranium-rich primary minerals are naturally less abundant. Fig. 6a thus illustrates that the original lithology constitutes the primary controlling factor

International Journal of Scientific Engineering and Science
Volume 10, Issue 5, pp. 31-43, 2026. ISSN (Online): 2456-7361

for the presence of uranium in the district's soils, preceding the influence of surface weathering processes.

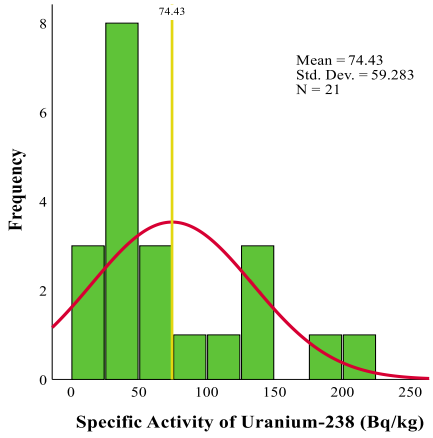

Fig. 4a. Frequency distribution of ^{238}U series activities

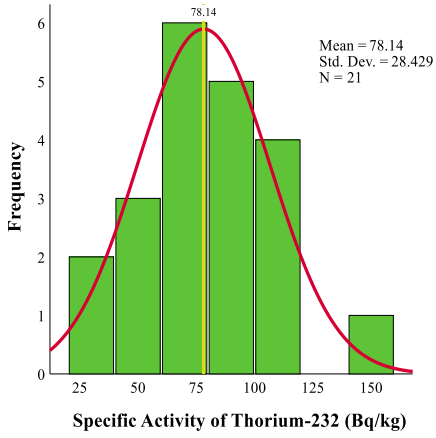

Fig. 4b. Frequency distribution of ^{232}Th series activities

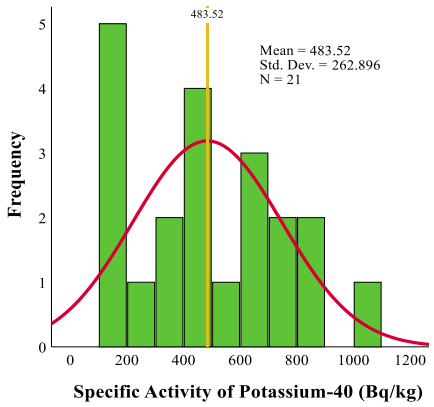

Fig. 4c. Frequency distribution of ^{40}K activities

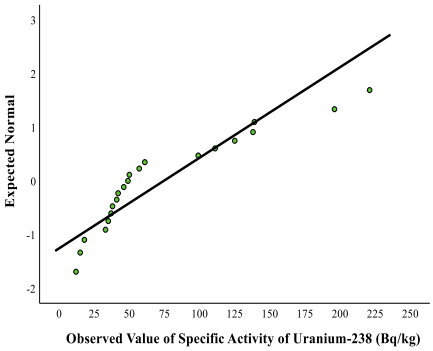

Fig. 5a. Normal Q-Q Plot of ^{238}U series activity concentrations

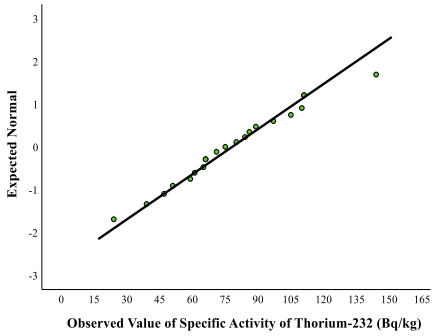

Fig. 5b. Normal Q-Q Plot of ^{232}Th series activity concentrations

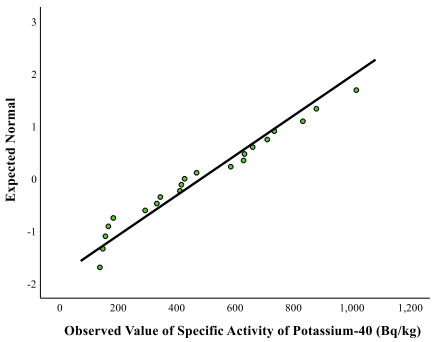

Fig. 5c. Normal Q-Q Plot of ^{40}K activity concentrations

The mapping presented in Fig. 6b provides a visual understanding of the spatial distribution of ^{238}U specific activities across the entire territory, where each measurement point corresponds to one of the 19 communes of the Vohémar district identified in Fig. 1. The map reveals a marked spatial heterogeneity, with a gradient of ^{238}U specific activities increasing from the eastern coastal communes, such as Vohemar, Ampanefena, and Fanambana, toward the inland areas located in the west and center. The intense red zones in Fig. 6b, indicating ^{238}U specific activities exceeding 200 Bq·kg^{-1}, clearly identify radiological hotspots localized mainly in the western part of the district, covering the communes of Andrafainkona (where point ECH-06 is located) and Ambinanin'andravory.

These high-radioactivity zones contrast sharply with the eastern and northern borders, represented in blue on the map, where ^{238}U specific activities remain at low levels between 20 and 40 Bq·kg^{-1} within the communes of Maromokotra, Bobakindro, Ampisikina, and Ampondra. This spatial structuring confirms that the western part of the district, also encompassing the communes of Daraina and Milanoa, characterized by more rugged terrain and plutonic geology, constitutes the region's primary uraniferous province. The extent of the yellow and green transition zones, affecting the communes of Tsarabaria, Antsirabe Nord, and Ambodisambalahy, shows a moderate diffusion of uranium around the main centers, likely due to sedimentary transport by hydrographic networks draining the basement toward the coastal plains of Ambalasatrana and Andravory.

Overall, the results presented in Fig. 6a and Fig. 6b, supported by Fig. 1, demonstrate that the spatial distribution of ^{238}U in the soils of the Vohémar district is a direct expression of its geological complexity. Ancient plutonic formations located in the western communes dictate the location of high radioactive activity points, while coastal communes benefit from a lower radiological environment due to the diluting role of sedimentary deposits.

3.3.2. Analysis of ^{232}Th Distribution Relative to the Geological Setting

Analysis of Fig. 7a highlights a close relationship between the specific activities of thorium-232 (^{232}Th) and the lithological composition of the district. High thorium activities overlap almost perfectly with the Neoproterozoic plutonic formations (Bemarivo belt) and the metamorphic complexes of the Daraina Group. Since thorium is an extremely stable element with low mobility under the pH conditions typically found in soils, its presence serves as a direct indicator of the parent rock mineralogy. As shown in Fig. 7a, high-content areas coincide with sectors rich in heavy accessory minerals such as

International Journal of Scientific Engineering and Science
Volume 10, Issue 5, pp. 31-43, 2026. ISSN (Online): 2456-7361

monazite and zircon, which are the primary hosts of thorium in Madagascar's crystalline basement. Unlike uranium, thorium does not undergo significant chemical transport, which explains why its distribution, although elevated, faithfully follows the contours of the district's deep geological structures.

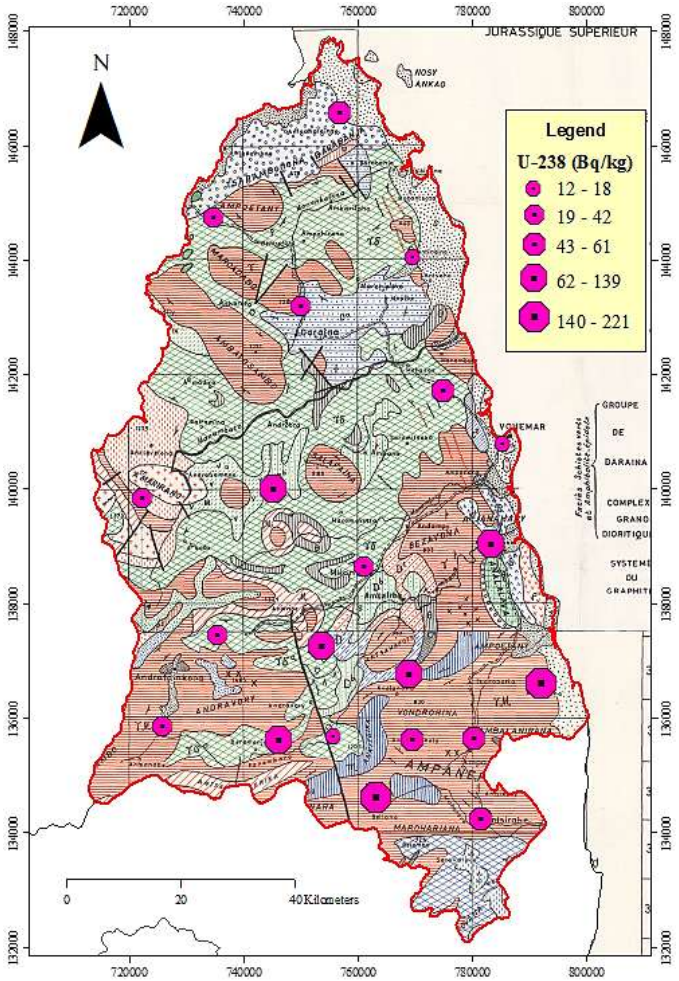

Fig. 6a. Geology and variation of ^{238}U activity

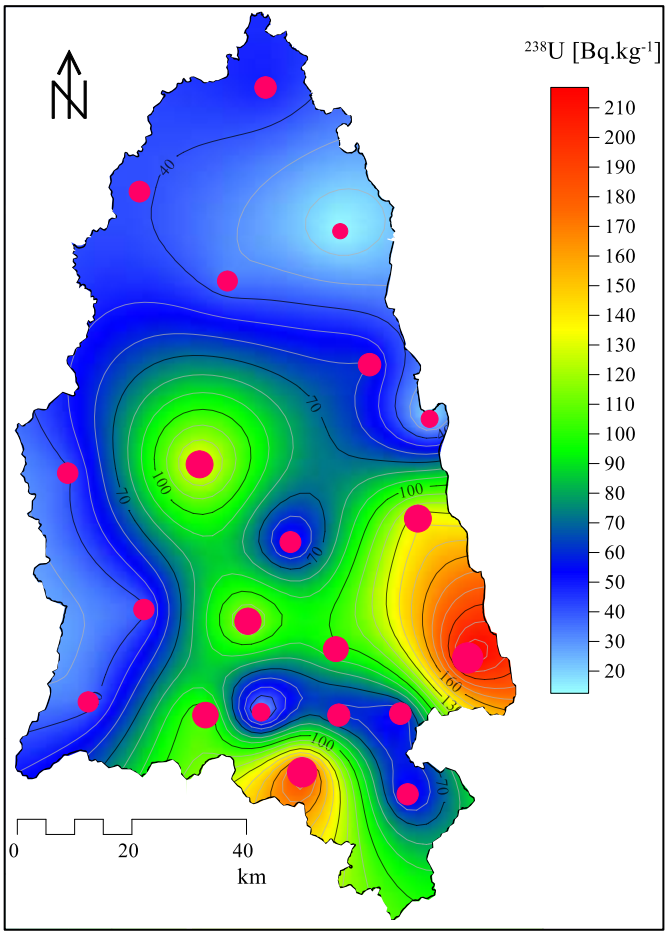

Fig. 6b. Distribution of ^{238}U in the soil of the Vohemar District

Fig. 6. Impact of geological formations on the specific activity of the ^{238}U series in volcanic soils of the Vohemar District

Fig. 7b, illustrating the spatial distribution of ^{232}Th specific activities, reveals a radiological landscape marked by a predominance of high activities in the central and southwestern parts of the district. Warning zones (colored red and orange) are identified where ^{232}Th specific activities exceed 120 Bq·kg^{-1}, which is four times the UNSCEAR world average. These hotspots are primarily concentrated in the rural communes of Andrafainkona, including point ECH-18 with its maximum activity of (144 ± 5) Bq·kg^{-1} Milanoa, and Ambinanin'andravory. These communes constitute the heart of the district's thoriferous province. Conversely, the blue zones on Fig. 7b, corresponding to more moderate ^{232}Th specific activities between 25 and 50 Bq·kg^{-1}, extend along the coastal fringe and toward the north, encompassing the communes of Maromokotra, Bobakindro, Vohemar, and Ampanefena.

The spatial transition shown by the green and yellow zones in Fig. 7b crosses the communes of Antsirabe Nord, Tsarabaria, and Ampisikina, indicating a consistent but less concentrated thorium presence in transition soils and fluvial alluvial deposits. The fact that thorium follows a normal statistical distribution (p = 0.965 in Table II) is visually reflected by a smoother and more homogeneous map than that of uranium, reflecting a powerful and ubiquitous natural geochemical background in the bedrock of inland communes such as Daraina and Ambodisambalahy.

Overall, the results obtained from Fig. 7a and Fig. 7b confirm that thorium-232 is the primary contributor to the elevated terrestrial radioactivity in the Vohemar district. Its spatial distribution is strictly controlled by the crystalline lithology of the western and central communes, establishing these sectors as areas with a very significant natural radiological background compared to international standards.

3.3.3. Analysis of ^{40}K Distribution Relative to the Geological Setting

Analysis of Fig. 8a reveals a striking correlation between potassium-40 (^{40}K) activities and pedogenesis processes governed by the district's geology. Since potassium is a major constituent of K-feldspars and micas, its presence is initially linked to the felsic magmatic rocks of the basement, such as granodiorites and gneisses. However, in contrast to uranium

International Journal of Scientific Engineering and Science
Volume 10, Issue 5, pp. 31-43, 2026. ISSN (Online): 2456-7361

and thorium, Fig. 8a illustrates that lithology is not the sole controlling factor. It is observed that high ^{40}K specific activity points are preferentially located in the rugged relief areas of the West, where soils are younger and primary minerals are less weathered. Conversely, the eastern plains and plateaus show marked depletion, as potassium is an extremely mobile element, easily leached by heavy tropical rainfall during the transformation of rocks into ferrallitic soils (laterites).

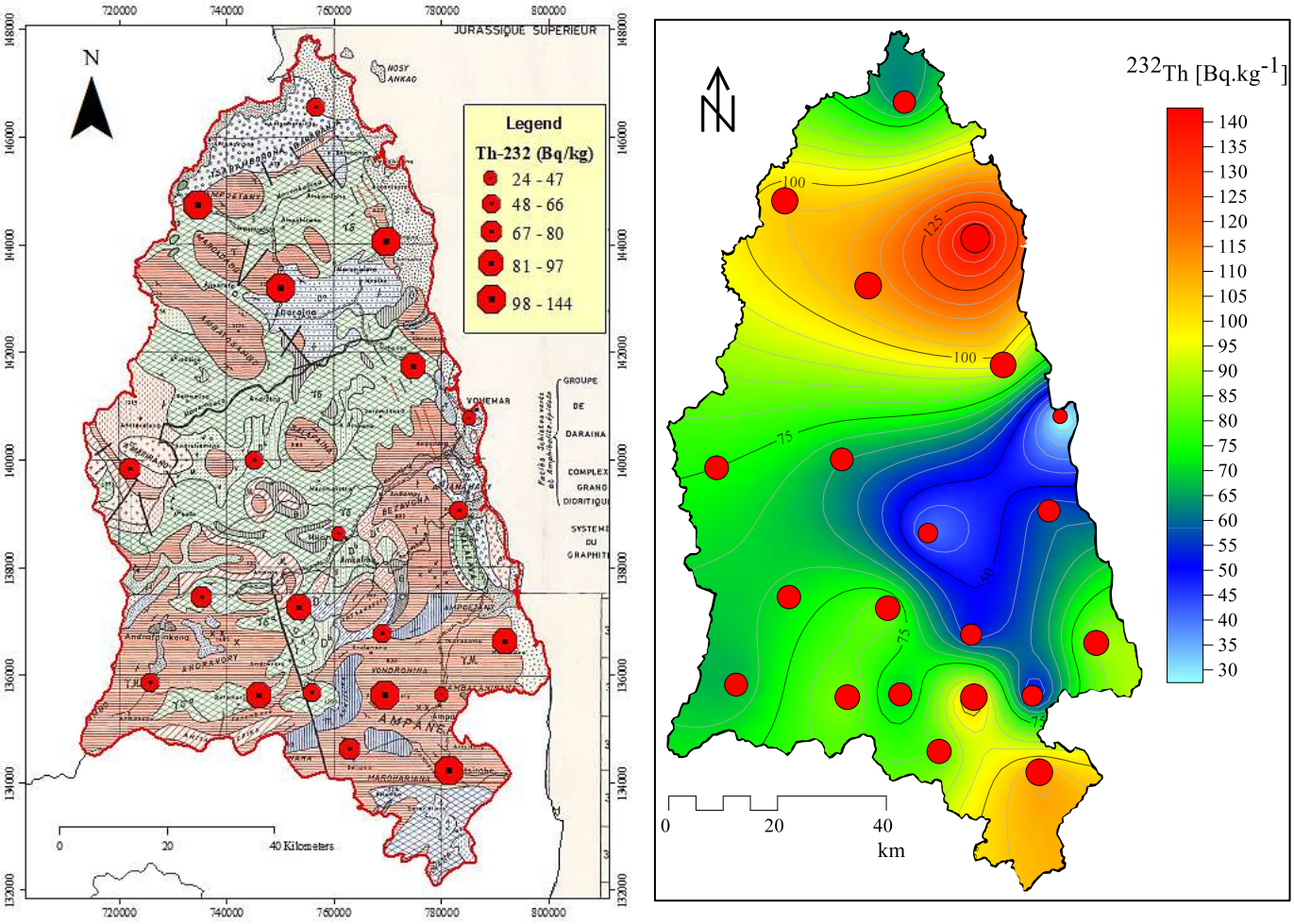

Fig. 7a. Geology and variation of ^{232}Th activity

Fig. 7b. Distribution of ^{232}Th in the soil of the Vohemar District

Fig. 7. Impact of geological formations on the specific activity of the ^{232}Th series in volcanic soils of the Vohemar District

The spatial mapping presented in Fig. 8b highlights a particularly sharp ^{40}K specific activity gradient between the West and East of the district. Intense red and orange zones, signaling very high ^{40}K specific activities between 800 and 1015 $Bq \cdot kg^{-1}$, are concentrated exclusively in the western and southwestern parts. These exceptional concentrations, well above the UNSCEAR world average (400 $Bq \cdot kg^{-1}$), are located in the rural communes of Andrafainkona, including point ECH-19 at (1015 ± 18) $Bq \cdot kg^{-1}$, Milanoa, Daraina, and Ambinanin'andravory. In these sectors, the proximity to the bedrock and less advanced chemical weathering allow for the preservation of significant potassium levels in the soils.

In contrast, Fig. 8b shows a vast blue area covering the entire eastern and northern half of the district, where activities drop radically below 300 $Bq \cdot kg^{-1}$, or even below 150 $Bq \cdot kg^{-1}$ in certain coastal sectors. This severe depletion affects the communes of Vohemar, Ampanefena, Fanambana, Maromokotra, Bobakindro, and Ampisikina. In these communes, the soils have undergone intense and prolonged leaching, leading to the mobilization of potassium toward the groundwater and leaving residual (lateritic) soils almost devoid of ^{40}K. Transition zones (green and yellow) cross the communes of Tsarabaria, Antsirabe Nord, Ambalasatrana, and Ambodisambalahy, marking the boundary between the mineral soils of the interior and the exhausted soils of the coastal fringe.

Overall, the results illustrated in Fig. 8a and Fig. 8b demonstrate that potassium-40 is the best indicator of the soil weathering status in the Vohemar district. Its spatial distribution, marked by a very distinct East-West duality, results from the antagonism between the mineralogical heritage of the western communes and the aggressive tropical leaching that characterizes the eastern coastal communes. The district thus exhibits zones of exceptional potassic richness inland, contrasting with a widespread deficiency along the coastline.

International Journal of Scientific Engineering and Science
Volume 10, Issue 5, pp. 31-43, 2026. ISSN (Online): 2456-7361

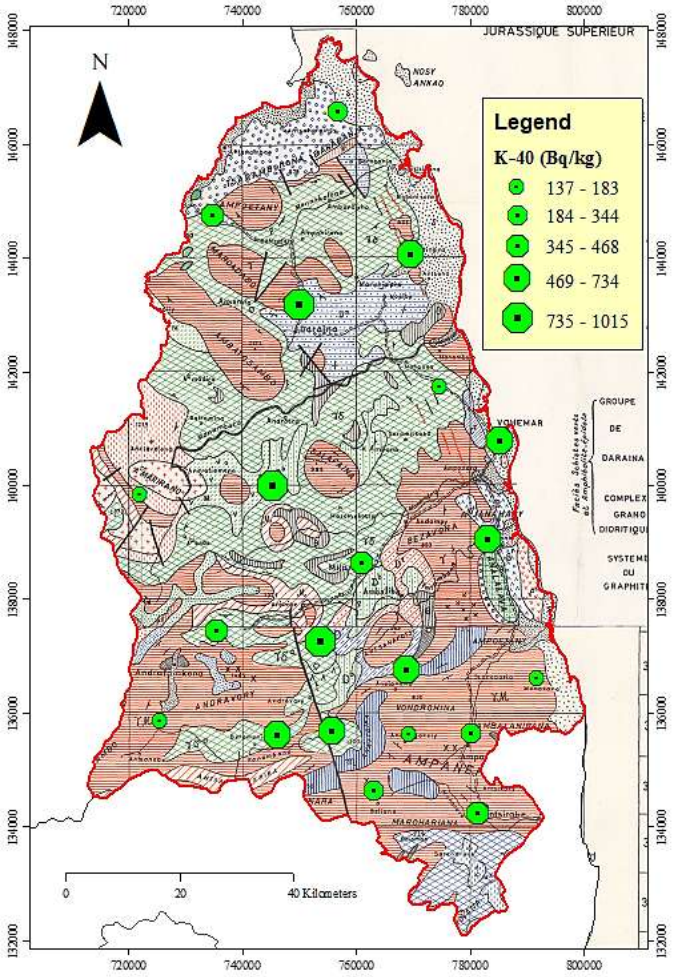

Fig. 8a. Geology and variation of ^{40}K activity

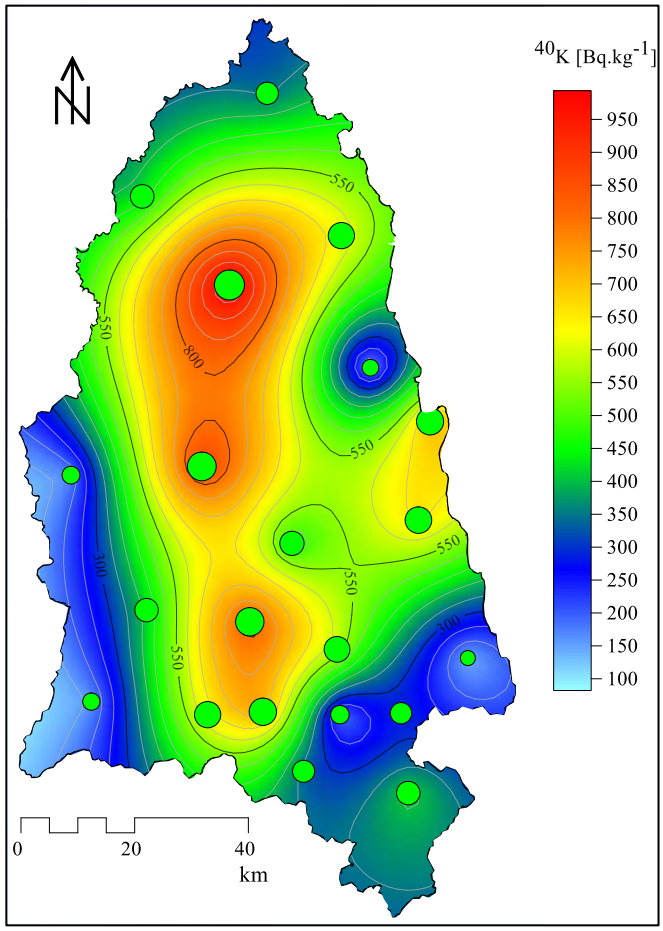

Fig. 8b. Distribution of ^{40}K in the soil of the Vohemar District

Fig. 8. Impact of geological formations on the specific activity of the ^{40}K in volcanic soils of the Vohemar District

3.4. Correlation Analysis and Geochemical Behavior of Radionuclides

Analysis of the relationship between uranium-238 and potassium-40, as illustrated in Fig. 9, reveals a total lack of linear correlation, with an extremely low coefficient of determination ($R^2 = 0.0027$).

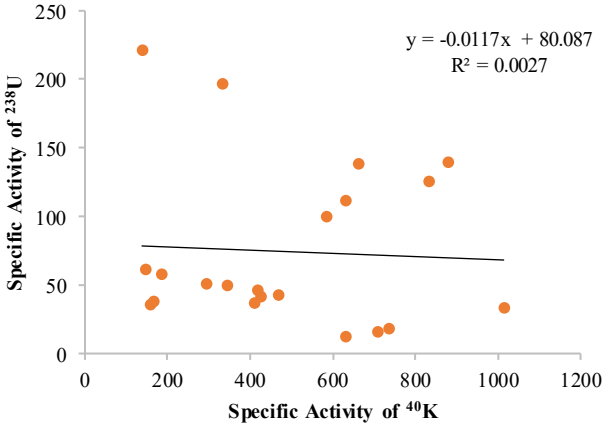

Fig. 9. Correlation between ^{238}U and ^{40}K in soils from the Vohemar District.

The regression line equation ($y = -0.0117x + 80.087$) exhibits a near-zero slope, indicating that the presence of uranium in Vohemar soils is statistically independent of potassium levels. This result corroborates the interpretations of Fig. 6b and Fig. 8b, confirming that these two elements are governed by distinct controlling mechanisms. While uranium remains primarily linked to the mineralogical heritage of the crystalline basement, potassium is drastically redistributed by climatic leaching. This geochemical decoupling suggests that surface weathering processes have erased any original magmatic relationship between these two elements.

Fig. 10 presents the correlation study between thorium-232 and uranium-238, which also results in a negligible R^2 coefficient of 0.0013 ($y = -0.0173x + 79.43$). From a geochemical perspective, this result is particularly significant because, in fresh and unweathered magmatic rocks, uranium and thorium typically exhibit a strong positive correlation due to their properties as incompatible elements. The lack of correlation observed here indicates a disruption of the original geochemical equilibrium during soil formation. As previously analyzed for Fig. 6 and Fig. 7, this decoupling is explained by the difference in mobility between the two nuclides: uranium

International Journal of Scientific Engineering and Science
Volume 10, Issue 5, pp. 31-43, 2026. ISSN (Online): 2456-7361

can be oxidized and transported in soluble form by seepage water, whereas thorium remains immobile, trapped within resistant heavy minerals. Consequently, the uranium hotspots identified in the western communes do not necessarily coincide with the maximum values of thorium specific activities, confirming selective redistribution during pedogenesis.

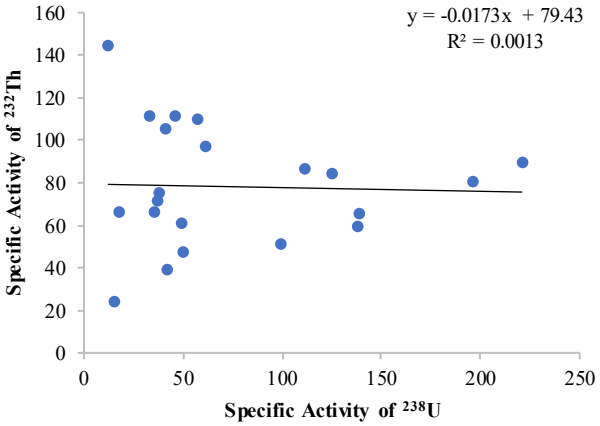

Fig. 10. Correlation between ^{232}Th and ^{238}U in soils from the Vohemar District.

Similarly, the correlation between thorium-232 and potassium-40, examined in Fig. 11, confirms this trend with an $R^2 = 0.0014$ $(y = -0.0041x + 80.106)$. This total independence between thorium a marker of mineralogical stability (Fig. 7b) and potassium a marker of weathering intensity (Fig. 8b) highlights the complexity of the soils in Vohemar. The processes that enrich the soil in thorium through the mechanical concentration of heavy minerals are entirely distinct from those that deplete the soil of potassium through chemical leaching. The dispersion of data points across the three correlation plots shows that each commune in the district possesses its own radiological signature, resulting from a unique blend of plutonic parent rock input and the local impact of the tropical climate.

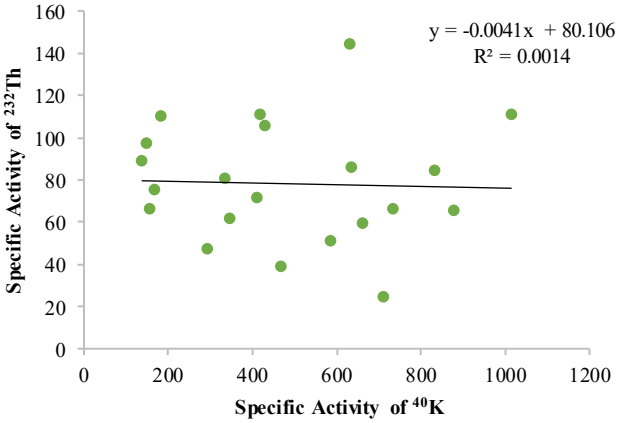

Fig. 11. Correlation between ^{232}Th, and ^{40}K in soils from the Vohemar District.

Overall, the study of correlations across Fig. 9, Fig. 10, and Fig. 11 demonstrates that natural radionuclides in the Vohemar district act as independent tracers of the district's geochemical history. The absence of a generalized linear correlation proves that these are mature and evolved soils, where secondary weathering processes have superseded the primary mineralogical signature of the basement rocks.

3.5. Comparison with Similar Studies in Madagascar

A comparison of the mean specific activities obtained in the Vohémar district (74 Bq·kg^{-1} for ^{238}U, 78 Bq·kg^{-1} for ^{232}Th, and 484 Bq·kg^{-1} for ^{40}K) with data from Table III reveals that this region possesses one of the highest radiological signatures in Northern Madagascar.

Firstly, radioactivity levels in Vohémar are significantly higher than those in neighboring districts within the SAVA and Diana regions. Compared to the Ambilobe district, where mean activities are only 18 Bq·kg^{-1} for ^{238}U and 40 Bq·kg^{-1} for ^{232}Th (Stolerie *et al.*, 2021), Vohemar exhibits concentrations two to four times higher. A similar observation is made for the Antalaha district, whether in its coastal zone of Ambohitralanana (34 Bq·kg^{-1} for ^{238}U and 38 Bq·kg^{-1} for ^{232}Th) according to Barijaona *et al.* (2017), or more generally across the entire district (33 Bq·kg^{-1} for ^{238}U and 54 Bq·kg^{-1} for ^{232}Th) according to Ngoko *et al.* (2024). This discrepancy is explained by the nature of the geological substrate: while Antalaha and Ambilobe are dominated by sedimentary formations or highly evolved ferrallitic soils, the Vohemar district rests on a granitic and metamorphic crystalline basement much richer in primary radioelements.

TABLE III. Comparison with a similar study on natural radioactivity in Madagascar soils

Locality	Average Specific activity (Bq/kg)		
	^{238}U	^{232}Th	^{40}K
Vohemar District (Present Study)	74	78	484
Ambilobe District (Stolerie et al., 2021)	18	40	518
Antalaha-Ambohitralanana littoral zone (Barijaona et al., 2017)	34	38	300
Antalaha District (Ngoko et al., 2024)	33	54	277
Antsiranana II District (Tsilailay et al., 2025)	48	61	194
Amber Mountain, Antsiranana II (Donné et al., 2021)	44	90	218
Ramena beach, Antsiranana II (Kall et al., 2014)	109	77	198
Baie des Français littoral zone, Antsiranana I (Kall et al., 2015)	139	126	313
Nosy-Be District (Djaovagnono et al., 2025)	33	39	138
Ambanja city and its Surroundings (Rahelivao et al., 2023)	44	123	730
Ampasindava peninsula, Ambanja (Rafidimanantsoa, 2021)	76	261	355
Befandriana Nord District (Randrianarivo et al., 2017)	21	198	200

Vohemar also stands out when compared to volcanic massifs and northern islands. Soils in the Nosy-Be district (33 Bq·kg^{-1} for ^{238}U, 39 Bq·kg^{-1} for ^{232}Th, and 138 Bq·kg^{-1} for ^{40}K), studied by Djaovagnono *et al.* (2025), appear severely depleted compared to those in Vohémar, reflecting more advanced leaching and ferrallitization on Nosy-Be. Similarly, although Montagne d'Ambre in the Antsiranana II district shows a notable thorium-232 activity of 90 Bq·kg^{-1} (Donné *et al.*, 2021),

its uranium-238 (44 Bq·kg^{-1}) and potassium-40 (218 Bq·kg^{-1}) activities remain well below the values measured in Vohemar.

However, the Vohemar district is not the most radioactive area in the Antsiranana province. Coastal sites rich in mineralized sands exhibit many more critical activities. This is the case for Ramena beach (109 Bq·kg^{-1} for ^{238}U) according to Kall *et al.* (2014) and, most notably, the coastal zone of the Baie des Français (139 Bq·kg^{-1} for ^{238}U and 126 Bq·kg^{-1} for ^{232}Th) according to Kall *et al.* (2015). These exceptional levels result from the mechanical concentration of heavy minerals (monazite, zircon, ilmenite) by wave and current action a densimetric sorting process that is more efficient than the *in-situ* weathering of soils in the Vohémar district.

Furthermore, a comparison with the city of Ambanja and its surroundings (Rahelivao *et al.,* 2023) shows that this area possesses higher thorium (123 Bq·kg^{-1}) and potassium (730 Bq·kg^{-1}) contents than Vohemar, although its uranium activity is lower (44 Bq·kg^{-1}). This disparity highlights the variability of magmatic sources in Madagascar, where some areas are preferentially enriched in thorium (Ambanja district) while others exhibit a more pronounced balance between uranium and thorium (Vohemar district).

Overall, this study confirms that the Vohémar district constitutes a major positive radiological anomaly compared to the surrounding sedimentary and volcanic districts (Antalaha, Ambilobe, Nosy-Be). While its levels remain below the coastal "hotspots" of Antsiranana (Baie des Français, Ramena), Vohémar establishes itself as a reference zone for the study of natural radioactivity linked to Madagascar's ancient crystalline basement.

IV. Conclusion

This study has provided the first comprehensive and in-depth characterization of natural radioactivity from the ^{238}U and ^{232}Th decay series and ^{40}K in the soils of the Vohemar district. The results reveal that this district is a major radiological province in Northern Madagascar, with mean specific activities for uranium-238 (74.43 ± 12.94 Bq·kg^{-1}) and thorium-232 (78.14 ± 6.20 Bq·kg^{-1}) reaching more than double the world averages prescribed by UNSCEAR (2000). Statistical analysis highlighted a marked spatial heterogeneity, revealing the existence of radiological hotspots, particularly in the western part of the district.

Radiological mapping demonstrated that the distribution of these radionuclides is the result of an interplay between a rich geological heritage, linked to the crystalline basement of the Bemarivo belt, and intense tropical weathering processes. Uranium and thorium appear as faithful markers of plutonic lithology, while potassium-40 serves as a tracer for climatic leaching, showing a striking duality between inland and coastal communes. The lack of correlation between the three elements confirms a decoupling of geochemical equilibrium, reflecting the maturity of the soils and the intensity of post-magmatic redistribution processes.

In conclusion, these results provide an indispensable reference database for the establishment of Madagascar's national radiological mapping. They also offer valuable indicators for environmental management and monitoring, radiation protection for resident populations, and the understanding of pedogeochemical dynamics in humid tropical environments. This study paves the way for subsequent exposure dose assessments to ensure the sustainable and safe management of natural resources in the SAVA region.

Acknowledgment

Acknowledgment is gratefully made to the Nuclear Techniques and Analysis department at INSTN-Madagascar and the Nuclear Metrology and Environment department at the University of Antsiranana for their significant contributions and technical guidance throughout this research.

References

[1] UNSCEAR. Sources and effects of ionizing radiation, Vol. 1. United Nations Scientific Committee on the Effects of Atomic Radiation. Report of the General Assembly with Scientific Annexes. United Nations, New York; 2000.

[2] Z. Donné, M. Rasolonirina, H.C. Djaovagnono, B. Kall, N. Rabesiranana & J. Rajaobelison. Study of water radioactivity transfer from telluric origin in the Amber Mountain, Antsiranana, Madagascar. *Scientific African*; 13 (2021): e00902.

[3] A.F. Barijaona, F. Asimanana & M. Rasolonirina. Contribution à l'étude de la radioactivité naturelle, par spectrométrie gamma, du sol dans la zone littorale d'Antalaha-Ambohitralanana Madagascar. *Afrique Science*, Vol. 13, No. 2, 2017.

[4] N. Rabesiranana. Contribution à l'étude de la radioactivité environnementale à Madagascar : de la quantification à l'utilisation des traceurs radio-isotopiques environnementaux. *HDR, Université d'Antananarivo, Madagascar*, pp. 1-140, 2017. http://biblio.univ-antananarivo.mg/pdfs/rabesirananaNaivo1_PC_HDR_17.pdf

[5] F. Ngoko, A. F. Solonjara, Z. Donné, D. Rasolozafy, and B. Kall. Étude de la radioactivité naturelle du sol : Cas du district d'Antalaha, région de SAVA, nord-est de Madagascar. *American Journal of Innovative Research and Applied Sciences*. Vol. 19, No 4, pp. 27-38, 2024. Doi: https://doi.org/10.5281/zenodo.13844565

[6] J. E. Rahelivao, Z. Donné, A. Razafindrapata, A. I. Joelisoafara, M. Rasolonirina & B. Kall. Study of Natural Radioactivity Levels and the Associated Radiological Hazards in Soil from Ambanja City and its Surroundings, Madagascar. *International Journal of Innovative Research in Science, Engineering and Technology*. Vol. 12, Issue 5, 2023. DOI:10.15680/IJIRSET.2023.1202005

[7] P. Chiozzi, P. De Felice, A. Fazio, V. Pasquale, M. Verdoya. Laboratory application of NaI(Tl) γ-ray spectrometry to studies of natural radioactivity in geophysics, Applied Radiation and Isotopes, Vol. 53, Issues 1–2, pp. 127-132, 2000. https://doi.org/10.1016/S0969-8043(00)00123-8.

[8] B. Kall, Z. Donné, M. Rasolonirina, N. Rabesiranana & G. Rambolamanana. Contribution à l'étude de la radioactivité gamma du sable des plages de Ramena et d'Orangea, Antsiranana, Madagascar. *Afrique Science*. Vol. 10, No. 4, pp. 23- 35, 2014.

[9] G. Cinelli, L. Tositti, D. Mostacci, J. Baré. Calibration with MCNP of NaI detector for the determination of natural radioactivity levels in the field. Journal of Environmental Radioactivity; Vol. 155–156, pp. 31-37, 2016, https://doi.org/10.1016/j.jenvrad.2016.02.009.

[10] J. P. Stolerie, M. Rasolonirina, Z. Donné, B. Kall & N. Rabesiranana. Etude de la radioactivité naturelle d'origine tellurique du district d'Ambilobe, Madagascar. *American Journal of Innovative Research Applied Sciences*. Vol. 13, No. 5, pp. 518-529, 2021.

[11] O. Rafidimanantsoa, M. Rasolonirina, Z. Donné, P. H. Ralaiarison, S. Tonissa, N. Rabesiranana & R. J. L. Zafimanjato. Caractérisation de la radioactivité naturelle du gisement des terres rares, de la presqu'île d'Ampasindava du nord-ouest de Madagascar. *American Journal of Innovative Research Applied Sciences*. Vol 13, No. 4, pp. 452-461, 2021.

[12] A. Randrianarivo, F. Asivelo Solonjara & F. Asimanana. Contribution à l'étude de la radioactivité du sol de district de Befandriana-Nord, Madagascar. *American Journal of Innovative Research and Applied Sciences.* Vol. 4, No. 1, pp. 22-28, 2017.

[13] B. Kall, T. Tombo, M. Rasolonirina, N. Rabesiranana & G.

Rambolamanana. Contribution à l'étude de dose due à la radioactivité gamma du sol sur la rive de la baie des Français, Antsiranana, Madagascar. *Afrique Science*, ISSN 1813-548X, Vol. 11, No. 1, pp. 122-135, 2015.

[14] Schreurs, G. & Rakotoarisoa, J.-A. (2011). The archaeological site at Vohemar in a regional geographical and geological context. Études océan Indien, 46-47. https://doi.org/10.4000/oceanindien.1169

[15] A. S. Kanmi, U. Ibrahim, N. G. Goki, U. Rilwan, M. I. Sayyed, Y. Maghrbi, B. F. Namq, L. A. Najam & T. Y. Wais. Assessment of natural radioactivity and its radiological risks in the soil of local government areas (Asa, Ilorin East, Ilorin South, Irepodun, Moro, and Oyun) in Kwara State, Nigeria. Case Studies in Chemical and Environmental Engineering. Vol. 11, 2025. DOI: 10.1016/j.cscee.2024.101040

[16] IRSN et INRS. (2014). Radioprotection : Radionucléides - Uranium naturel (Fiche ED 4321). Institut de Radioprotection et de Sûreté Nucléaire (IRSN) et Institut National de Recherche et de Sécurité (INRS), Paris, France. 12 p.

[17] IRSN et INRS. (2013). Radioprotection : Radionucléides - Thorium-232 (Fiche ED 4317). Institut de Radioprotection et de Sûreté Nucléaire (IRSN) et Institut National de Recherche et de Sécurité (INRS), Paris, France. 12 p.

[18] H. C. Djaovagnono, Z. Donné, M. Rasolonirina, A. F. Solonjara & B. Kall. Spatial Distribution of Natural Radioactivity from the ^{238}U and ^{232}Th Decay Series, and ^{40}K in the Volcanic Soils of Nosy-Be Island, Madagascar. *International Journal of Scientific Engineering and Science*. Vol. 9, Issue 7, pp. 36-45, 2025.

[19] A. S. Tsilailay, Z. Donné, F. R. Randrianantenaina, A. F. Solonjara & F. Asimanana. Spatial Distribution of Natural Radioactivity in the Volcanic Soil of Antsiranana II District, Madagascar. International Journal of Scientific Engineering and Science. Vol. 9, Issue 8, pp. 26-35, 2025.

[20] S. Singh, A. Rani & R. K. Mahajan. ^{226}Ra, ^{232}Th and ^{40}K analysis in soil samples from some areas of Punjab and Himachal Pradesh, India using gamma ray spectrometry. *Radiation Measurements*. Vol. 39, Issue 4, pp. 431-439, 2005.

[21] Amanjeet, A. Kumar, S. Kumar, J. Singh, P. Singh & B. S. Bajwa. Assessment of natural radioactivity levels and associated dose rates in soil samples from historical city Panipat, India. *Journal of Radiation Research and Applied Sciences*. Vol. 10, Issue 3, pp. 283-288, 2017.

[22] M. A. Adabanija, O. N. Anie & M. A. Oladunjoye. Radioactivity and gamma ray spectrometry of basement rocks in Okene area, southwestern Nigeria. NRIAG *Journal of Astronomy and Geophysics*. Vol. 9, Issue 1, pp. 71-84, 2020.

[23] A. Durusoy & M. Yildirim. Determination of radioactivity concentrations in soil samples and dose assessment for Rize Province, Turkey. Journal of Radiation Research and Applied Sciences. Vol. 10, Issue 4, pp. 348-352, 2017.

[24] U. S. Chakma, J. C. Roy, C. Mondol, A. Chakrobortty & M. A. Hossain. Investigating the Spatial Distribution, Environmental Pathways, and Public Health Risks of Natural Radioactivity in Khulna Division, Bangladesh. Asian Journal of Applied Science and Technology. Vol. 10, Issue 1, pp. 13-36, 2026.

[25] L. A. Najam, T. Y. Wais, Y. Y. Kassim, B. F. Namq, F. M. A. Al-Jomaily, A. Saleh, M. I. Sayyed, S. Nazir, H. M. Ahmed & M. S. Khan. Radiological hazard assessment of ^{226}Ra, ^{232}Th, and ^{40}K in soil samples collected from northwestern Iraq. International Journal of Environmental Analytical Chemistry. DOI: 10.1080/03067319.2025.2553749, 2025.

[26] M. Tzortzis, H. Tsertos, S. Christofides, G. Christodoulides. Gamma-ray measurements of naturally occurring radioactive samples from Cyprus characteristic geological rocks. Radiation Measurements, Vol. 37, Issue 3, pp. 221-229, 2003. https://doi.org/10.1016/S1350-4487(03)00028-3.

[27] A.D. Bajoga, A.N. Al-Dabbous, A.S. Abdullahi, N.A. Alazemi, Y.D. Bachama, S.O. Alaswad, Evaluation of elemental concentrations of uranium, thorium and potassium in top soils from Kuwait. *Nuclear Engineering and Technology*, Vol. 51, Issue 6, pp. 1638-1649, 2019. https://doi.org/10.1016/j.net.2019.04.021

[28] P. Shaba, K. K. Maseka, and P. Hayumbu. Evaluation of Radiological Risk Hazards in Sediments and Selected Streams Around Kalulushi and Kitwe Towns. *Archives of Microbiology and Immunology*, Vol. 8, Issue 4, pp. 472-479, 2024. DOI: 10.26502/ami.936500194

[29] G. Erdi-Krausz, M. Matolin, B. Minty, J. P. Nicolet, W. S. Reford & E. M. Schetselaar. *Guidelines for radioelement mapping using gamma ray spectrometry data: also, as open access e-book*. (IAEA-TECDOC; Vol. 1363). International Atomic Energy Agency (IAEA), 2003. http://wwwpub.iaea.org/MTCD/publications/PDF/te_1363_web.pdf

[30] M. Tzortzis, & H. Tsertos. Determination of Thorium, Uranium and Potassium Elemental Concentrations in Surface Soils in Cyprus. Journal of Environmental Radioactivity, Vol. 77, pp. 325-338, 2004. https://doi.org/10.1016/j.jenvrad.2004.03.014